Molecular dynamics simulations of Eu(NO3)3 salt with DMDOHEMA in n-alkanes: Unravelling curvature properties in liquid-liquid extraction

Simon Stemplinger, Magali Duvail, Jean-François Dufrêche

Version of Record: https://www.sciencedirect.com/science/article/pii/S0167732221027604
Manuscript_59bc1470be044619b245b6d51b4f6ea9

Molecular dynamics simulations of $Eu(NO_3)_3$ salt with DMDOHEMA in *n*-alkanes: Unravelling curvature properties in liquid-liquid extraction

Simon Stemplinger[a], Magali Duvail[a,*], Jean-François Dufrêche[a]

[a] *ICSM, Univ Montpellier, CEA, CNRS, ENSCM, Marcoule, France*

Abstract

The spontaneous packing parameter and the bending rigidity of small reverse aggregates similar to reverse micelles in different diluents have been investigated. The considered system consisting of a common extractant (DMDOHEMA), a lanthanide salt ($Eu(NO_3)_3$) and water in various *n*-alkanes (*n*-heptane, *n*-nonane and *n*-dodecane) has been studied using molecular dynamics simulations to the obtain penetration behavior of different diluents. Umbrella sampling and fluctuation theory have been used to yield the bending rigidity. Different approaches for the determination of the packing parameter have been applied. For the most reproducible methodology a spontaneous packing parameter of 4.6 and an effective rigidity constant of 50 k_BT per extractant molecule has been found.

Key words: solvent extraction, reverse micelles, curvature, fluctuations, molecular dynamics

Corresponding author
Email address: magali.duvail@cea.fr (Magali Duvail)

1. Introduction

The role of amphiphilic extractant molecules has been heavily studied in the last few decades since they are present in all the biphasic solvent extraction processes [1–6]. These extractant molecules allow the presence of hydrophilic and hydrophobic environments to coexist in a solution, usually by forming polydisperse aggregates in the complex organic phases [7–9]. Due to the metal-ligand nature interaction in those aggregates an extractant molecule can selectively bind the target metal ions and transport them into the organic phase, leaving the non-target ions in the aqueous phase [10]. Fully understanding the accurate solvation mechanism is the key of defining the complex energetics of solvent extraction and, *in fine*, improving separation efficiency [11, 12]. To achieve this, both, the long-range interactions making up the "soft matter" solution microstructure and the short-range interactions relevant for the ligand to metal binding, have to be addressed [13]. Despite the apparent disparity of the underlying factors, the combination of them is not only relevant for solvent extraction, but also synthesis of nanoparticles [14–16], and nanomedicine [17].

The solvent extraction chosen here for investigation is the one implying the extractant molecule *N,N'*-dimethyl-*N,N'*-dioctylhexylethoxymalonamide (DMDOHEMA), see figure 1. It is a representative of the broadly applied malonamide extractant family [18, 19], and is the current reference extractant in the DIAMEX (DIAMide EXtraction) process. This refers to the liquid-liquid solvent extraction for recovering selectively trivalent actinide (An^{3+}) and lanthanide (Ln^{3+}) cations from the PUREX (Plutonium and Uranium Refining by EXtraction) raffinate [20, 21]. Having empirical data from inves-

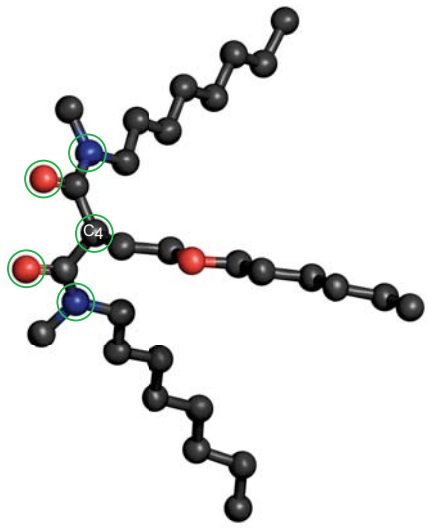

Figure 1: Representation of the malonamide extractant DMDOHEMA. The green circles indicate that the corresponding atoms belong to the micelle core.

tigations using structural and physical techniques [22–24], DMDOHEMA is a suitable candidate for molecular dynamics (MD) simulations.

In the extraction process, DMDOHEMA transfers cations to the organic phase by making aggregates similar to small reverse micelles [1, 7]. Except their small molecularities, such aggregates behave like reverse micelles since they have well-defined polar cores, and orientated apolar ring composed of extractant molecules (surfactants in the case of micelles). Furthermore, critical aggregation concentration (CAC) can be calculated, and curvature phenomenon of the hydrophobic chains is observed. Here, the polar core of these micelles consists of the metal cation, the counter ions, the co-extracted water and the polar part of the extractant molecules, while the apolar ring around is made up by the extractants hydrophobic chains. Generally speaking, the

extraction reaction follows the equation

$$M^{3+} + 3NO_3^- + xH_2O + y\bar{L} \rightleftharpoons \bar{A}, \tag{1}$$

where M^{3+} is the trivalent metal cation, L the free (neutral) DMDOHEMA molecule and A the formed (neutral) aggregate. The bar above the compound marks the species within the organic phase. The aggregation number y and the amount of co-extracted water x have been investigated experimentally [7, 8, 23, 25] and found to be dependent mainly on the concentrations of extractant and acid [26], as well as, of course, the metal cation extracted [27]. For extractant concentrations below 1 mol L^{-1} the aggregation number was found to be three or four, while at higher DMDOHEMA concentrations larger aggregates with up to ten amphiphiles molecules are formed. Additionally, it was found that low metal ion contents produce small reverse micelles containing one cation, whereas higher metal ion concentration favors a clustering of the micelles to polynuclear aggregates with bridged nitrate [2]. For instance, for low concentrations Ellis *et al.* found micelles with one Eu^{3+}, three nitrate, one water and three DMDOHEMA extractant molecules. Despite MD simulations proved themselves useful in validating those empirical studies on the aggregates, to our best knowledge, simulation methods have never been applied to investigate the influence of the diluent itself. For practical reasons, most MD simulations are carried out in a *n*-heptane as organic phase, although longer chained *n*-alkanes find more use in industrial applications [28]. This simplification might lead to wrong results from MD simulations as already observed for uranyl extraction with trioctylamine extractants under sulfuric conditions [29]. An explicit consideration of the diluent may both, help in validating former simulation data

and aid the research for more efficient extraction [30–33].

Based on those findings, it was the goal of this paper to investigate the influence of the diluent on micellar properties. Therefore, umbrella sampling molecular dynamics simulations were used in order to access the curvature and the packing parameter of reverse micelles composed of hydrated europium nitrate ($Eu(NO_3)_3$) and DMDOHEMA in a structure most relevant for low metal ion and extractant concentrations, as shown experimentally and theoretically [2]. Methodically, this was achieved by modifying the micelle core size through an external constraint.

The aim of this work is to better understand the parameters influencing the size of the polar core in extraction. Recent works have shown that it is possible to predict quantitatively the extraction by a model that effectively characterizes all the phenomena involved: complexation, ion concentration, interfaces, bending effects, etc [34, 35]. To model the extraction, we can then take into account all the species possibly present in the solvent phase and not only a representative sample of the chemistry. The interest of such an approach is that the collective effects, as *e.g.* synergy, appear naturally without having to reparameterize the system [4]. Nevertheless, some phenomena, such as the curvature effects that control the size of the species formed [36], require a parameterization that is difficult to know *a priori* and a study of these aggregation phenomena is important for the future development of these approaches. Several mesoscopic parameters can account for these curvature effects. One of them is the packing parameter p which has the advantage of being a molecular quantity which depends on the environment. Within this framework, in a complete theory all the equilibrium

properties can be calculated: Critical Aggregation Concentration (CAC) / Critical Micellar Concentration (CMC), extraction isotherms, structures (X-ray diffraction, SAXS, and SANS spectra) [37–41].

It should be emphasized that incorporating notions of soft matter and colloidal theories is in no way in opposition to the well-supported concepts of complexation or to the molecular effects of first spheres that can be described by molecular simulations. They simply allow to couple them with a more efficient consideration of the phenomena related to long-range interactions and configuration entropy.

Thus the interest of such an approach is to be able to propose a more complete modeling of the extraction where, instead of considering a small number of species representing on average the numerous chemical species present, one considers the whole set of possible stoichiometries by using these collective effects concepts of soft matter coming in particular from the theory of microemulsions. Such an approach has recently been able to successfully predict the extraction of rare earths [39, 40]. It does not contradict in any way the significance of complexation phenomena necessary for extraction, but they are coupled to other phenomena such as those of entropic nature related to the high concentration of polar heads or the effects of curvature of the chains.

The important point is that by definition these models which consider in some way the solvent phases as microemulsions *do not necessarily exhibit characteristic aggregate size or maximum in the distribution at the associated cluster numbers* contrary to what was written in a recent article [42]. Persistence length are not characteristic size of aggregates [6]. To simplify the

description of the phenomena, we simulated here by molecular dynamics the smallest aggregates comprising 3 or 4 extractant molecules. These species of lowest molecularity are the most common for dilute phases. The studies which model diluted suspensions, for states close to the critical aggregation concentration (CAC), logically focus on them. But one should not forget that if the concentration increases, the entropic cost to form aggregates decreases and structures of much higher molecularity appear [43], as the curvature can be adapted to very different geometries and sizes, as can be seen for instance in the study of viscosity [44].

The point that justifies the use of microemulsion models is therefore in no way the universal presence of aggregates of characteristic size. It is in fact more simply the presence of polar domains. It is even possible to propose flexible microemulsion models where the curvature term of the extractant molecule has only a marginal role. Except perhaps at the CAC, the size of the micelles is not directly controlled by the curvature effects, it depends rather on the entropic effects [45, 46].

2. Theory for curvature effects

While describing the elastic properties of lipid bilayers, Helfrich [47] used the formula

$$w_c(c_1 + c_2) = \frac{\kappa}{2}(c_1 + c_2 - 2c_0)^2 + \bar{\kappa} c_1 c_2 \qquad (2)$$

to give the curvature-elastic energy per unit area with c_1 and c_2 being the principal local curvatures, c_0 the spontaneous curvature, and κ and $\bar{\kappa}$ the bending and Gaussian rigidity constants. Applying the theory to a spherical

reverse micelle with the radius R gives us

$$c_1 = c_2 = c = \frac{1}{R}. \tag{3}$$

Only considering the curvature, the free energy of the micelle surface is then

$$F_c = \int w_c(c) \mathrm{d}S = 8\pi\kappa \left(1 - \frac{c_0}{c}\right)^2 + 4\pi\bar{\kappa} \tag{4}$$

where $\int \mathrm{d}S = 4\pi R^2$.

Originally describing bilayers and micelles in water and taking into account stretching, tilting and curvatures, the molecular theories were later linked to mesoscopic theories by Szleifer *et al* [48]. Being applicable in cases of small interfacial layer thickness or chain length, the theory proofed itself valuable for oil in water (o/w) microemulsions and sphere to cylinder transitions in water-based micelles for almost 30 years [49–51]. But this approach has only recently been applied for the first time in the case of weak reverse aggregates, that are present in liquid-liquid extraction using extractants like DMDOHEMA [52]. Based on the work of Israelachvili *et al.* [53], Duvail and co-workers described the total free energy of bending contribution as

$$F = N\frac{\kappa^*}{2}\left(p - p_0\right)^2, \tag{5}$$

where N is the total number of surfactant molecules involved in the micelle. p and p_0 are the effective and spontaneous packing parameter, respectively, and κ^* is the effective bending rigidity constant.

For spherical micelles a_0, the area of the interface between polar core and apolar chains, is given by

$$a_0 = 4\pi R^2. \tag{6}$$

Changing the radius by the length l changes the area according to

$$a(l) = 4\pi(R+l)^2 = a_0\left(1 + 2\frac{l}{R} + \frac{l^2}{R^2}\right), \tag{7}$$

and by integrating this equation we get the corresponding volume

$$v = \int a(l)\mathrm{d}l = a_0\left(l + \frac{l^2}{R} + \frac{l^3}{3R^2}\right), \tag{8}$$

where we consider l being the length of the hydrophobic chain L_s and, therefore, v the chain volume. The packing parameter p [53] is defined as

$$p = \frac{v}{a_0 L_s}. \tag{9}$$

Therefore, it is also accessible via

$$p = 1 + \frac{L_s}{R} + \frac{L_s^2}{3R^2}, \tag{10}$$

an equation that solely depends on L_s and R, which both are easily accessible from molecular dynamics simulations.

It should be noted that both, Eqns. 4 and 5, approach the same effect and, therefore, are globally similar, linking the effective rigidity constant κ^* to the bending and Gaussian rigidity constants, κ and $\bar{\kappa}$. However, the approaches differ in how the interface is considered since the Helfrich formalism assumes a infinite thin interface and the molecular model in terms of packing parameter introduces the thickness of the chain length L_s [36].

The present paper mainly focused on spherical reverse micelles since it correspond to the shape of the aggregates formed in this system. However, it should be noted that this theory, based on the packing parameter, has been first developed to predict the self-assembly of micellar aggregates having

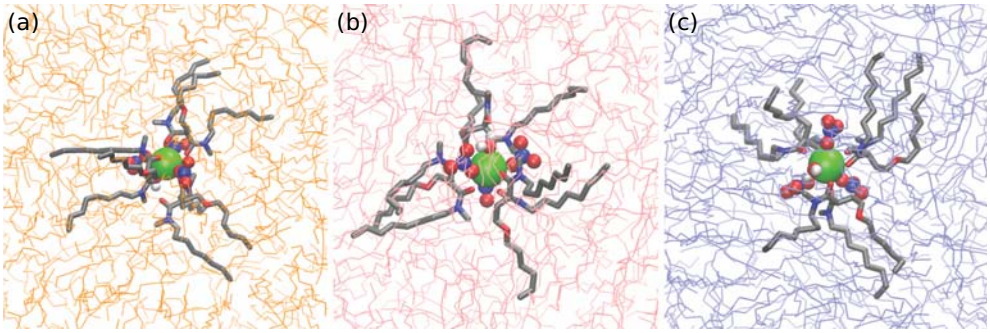

Figure 2: Snapshots of the MD simulation of the micelle composed of Eu^{3+} (green), three nitrate, water and three DMDOHEMA extractant molecules in (a) *n*-heptane (orange), (b) *n*-nonane (pink) and (c) *n*-dodecane (violet).

different shapes: spheres, ellipsoids, cylinders, bilayers [53]. Furthermore, Danov *et al.* recently demonstrated that such an approach could also be applied to predict the thermodynamics of wormlike micelles growth with non-ionic [45] and ionic surfactants [46].

3. Simulation details

3.1. Molecular dynamics simulations

Classical molecular dynamics (MD) simulations were performed in the NpT ensemble with SANDER14, a module of AMBER14 [54] using explicit polarization because of the presence of lanthanide cations [55–57]. Aggregates containing one europium cation Eu^{3+}, three nitrate anions NO_3^-, one water molecule and three DMDOHEMA extractant molecules were simulated in *n*-heptane, *n*-nonane and *n*-dodecane. For this, aggregates have been built from the stable experimental stoichiometry [2] and then solvated in 1000 *n*-alkanes (Fig. 2), as already done for other Ln^{3+} aggregates [52, 58]. The systems were equilibrated at 298.15 K and 1 bar for at least 200 ps. The

simulations were run for 5 ns solving the equations of motion with a 1 fs time step. Since aggregates are already formed, this simulation time is large enough to have good structural and thermodynamics aggregate solvation properties in n-alkanes as already done for others Ln^{3+}–containing aggregates [52, 58]. This simulation time allows also to calculate small fluctuations of the solvent density over the time, typically 0.002 g cm^3. The pressure was controlled by the weak-coupling Berendsen barostat with compressibilities of 144.0×10^{-6}, 117.7×10^{-6} and 98.8×10^{-6} bar^{-1} for n-heptane, n-nonane and n-dodecane, respectively [59, 60]. For the temperature also a weak-coupling algorithm was used. Periodic boundary conditions were applied to the simulation box. Long-range interactions have been calculated using the particle-mesh Ewald method [61].

The van der Waals force was described by a 12-6 Lennard-Jones (LJ) potential, where ε_{ij} and σ_{ij} were determined to reproduce experimental structural properties of molecules and ions in solution. Water molecules were described by the rigid POL3 model [62, 63] taking the polarization into account. LJ parameters used for the Eu^{3+} and the NO_3^- anions are described in Refs. [64] and [65], respectively. The polarizable force fields we recently developed for DMDOHEMA [52, 65] and the n-alkanes [29] have been used. These latter are based those developed by Siu et al. for long hydrocarbon chains [66]. Furthermore, atomic polarizabilities have been modified with respect to the ones determined from *ab initio* calculations by van Duijnen *et al.* [67]. All the parameters and the validation of the n-alkane force fields are given in the Supporting Information (Tables S1, S2 and S3, and Figure S1).

To visualize the trajectories the software VMD [68] was used. Further

Table 1: List of the reaction coordinate ξ_0

Diluent	ξ_0 / Å
n-heptane	5.0, 5.5, 5.75, 6.0, 6.5, 6.75, 7.0, 7.5, 8.0, 8.25, 8.5, 9.0, 9.25, 9.5, 9.75, 10.0
n-nonane	5.0, 5.25, 5.5, 6.0, 6.5, 6.75, 7.0, 7.5, 8.0, 8.25, 8.5, 9.0, 9.5, 10.0
n-dodecane	5.0, 5.5, 5.8, 5.9, 6.0, 6.5, 6.8, 7.0, 7.5, 8.0, 8.2, 8.5, 8.9, 9.2, 9.5, 9.7, 10.0

analysis heavily relied on the software CPPTRAJ, as well as its corresponding Python library PTRAJ [69], and on the MDAnalysis Python library [70, 71]. Additionally, the Python packages of the SciPy [72] ecosystem have been used in the processing of the simulation data.

3.2. Umbrella sampling

Potentials of mean force (PMF) of the reverse micelles have been calculated in *n*-heptane, *n*-nonane and *n*-dodecane using umbrella sampling (US) simulations in order to obtain the elastic properties of the interface between polar core and the apolar chains as a function of the diluent chain length. To achieve this, an umbrella spring force with a spring constant k of 10 kcal mol^{-1} Å^{-2} was pairwise applied between all three ternary carbon atoms of the diamide group of the DMDOHEMA molecules (named C4 in Fig. 1). The reaction coordinate ξ_0, corresponding to the C4 – C4 distance, was set to values between 5 and 10 Å with steps of 0.5 Å (Fig.3). To get optimal overlap of the equilibrium windows, additional distances were added (Figs. S2, S3 and S4). All ξ_0 values of the sampling simulations can be found in Table 1. For each window, the systems was equilibrated at 300 K for 50 ps, and then the production runs were performed in the NVT ensemble for 1 ns using a Langevin thermostat with a collision frequency of 25 ps^{-1}. Note that this

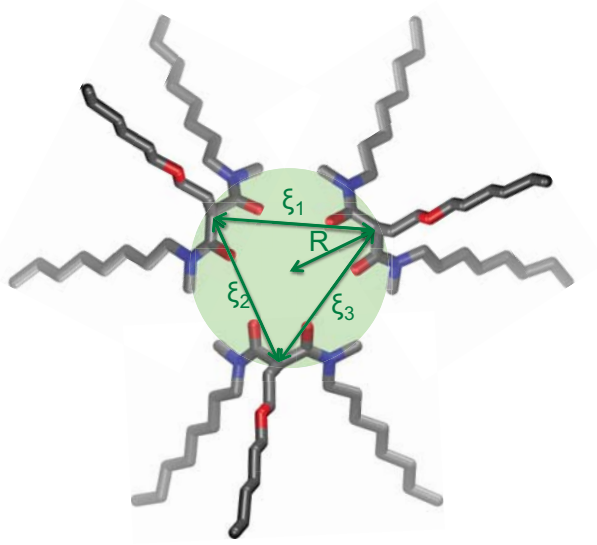

Figure 3: Schematic representation of the reverse micelle consisting of three DMDOHEMA molecules and containing the Eu^{3+} cation in the core. The reaction coordinate ξ_0 between the ternary carbon atoms of the diamide, depicted in dark green, was varied in the umbrella sampling MD simulations.

represents MD simulations of 16, 14 and 17 ns in *n*-heptane, *n*-nonane and *n*-dodecane, respectively. Then, free energy profiles were calculated using the weighted histogram analysis method (WHAM) [73, 74].

4. Results and discussion

4.1. Chain length

In order to access the packing parameter via Eqn. 10 the chain length of the extractant has to be known. Since it was found that the chain length is mostly independent of the reaction coordinate ξ_0 for micelles in a medium [52], the average length was calculated from the non-biased classical MD simulation and assumed to be alike for all umbrella sampling windows.

For the central chain of the DMDOHEMA molecule, the chain length was defined as the distance between the central ternary carbon atom C4 and the terminal carbon atom of the hexyl-ethoxy chain, whereas for the lateral chains it was defined as the distance between the nitrogen atoms and the terminal carbon atoms of the octyl chains. The value found for the end-to-end distance of the chains is 9.1 Å in all three diluents. Calculating the maximum extension via the Tanford's formula [75] ($l_{\max} = 1.5 + 1.265\ n_c = 11.6$ Å), considering the heteroatoms behave like carbon ($n_c = 8$), gives a extension of around 78 %.

In addition, the chain length, *i.e.*, the end-to-end distance, of the diluents themselves were investigated. Average chain lengths of 6.9, 9.0 and 12.1 Å were found for *n*-heptane, *n*-nonane and *n*-dodecane, respectively. Furthermore, the distribution of lengths was analyzed, (Fig. 4). For the *n*-alkanes three distinct peaks are observed in the distributions, which is due to the conformational isomers. The rightmost peak for each diluent represents a molecule with only anti conformations. Substituting one or more anti conformations with gauche conformations leads to shortening of the end-to-end distance.

The distribution of the DMDOHEMA chain length is mainly independent of the diluent. A good agreement between the distribution of *n*-nonane and DMDOHEMA is clearly seen.

4.2. Chain angle

To investigate the chain orientation, the angle between the terminal carbon of the hexyl-ethoxy chain of DMDOHEMA and the extended Eu-C4 distance was investigated from the non-biased MD simulations, with C4 be-

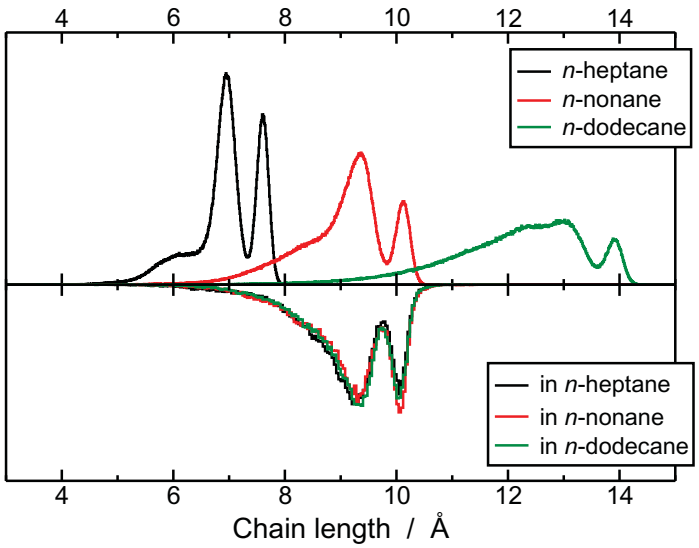

Figure 4: (Top) Distribution of chain length of the diluents n-heptane (black), n-nonane (red) and n-dodecane (green), and (Bottom) the DMDOHEMA chains in aggregates in the various diluents.

ing the marked carbon atom in figure 1. In figure 5 the angles are shown as a function of the Eu-C4 distance for n-heptane, n-nonane, and n-dodecane. In the left figures, the average values are shown as a red line in addition to the angles for the three extractant molecules in different colors, in the right the corresponding histograms are shown. Bidentate DMDOHEMA gives an Eu-C4 distance of approximately 4.2 Å, whereas monodentate gives approximately 4.8 Å. For the bidentate extractant the angular movement increases from n-heptane to n-dodecane and, therefore, the average angle decreases steadily. In contrast, the angle for the monodentate DMDOHEMA is more restricted for the longer chained diluent and the distribution gets narrower and moves towards higher $\cos\theta$ values. It appears that the penetrating n-heptane screens the chains against coalescence and the chains protrude radi-

ally.

In *n*-dodecane, one extractant molecule has been temporarily pushed into the second coordination sphere with a corresponding Eu-C4 distance of 6 Å. Here, the water molecule was located between the Eu^{3+} cation and the DMDOHEMA molecules for around 0.1 ns; this only occurred in *n*-dodecane.

4.3. Core area and micelle volume

In addition to the chain length, the core area and the apolar ring volume were investigated as they directly influence the packing parameter. To determine the core area the heteroatoms and the ternary carbon of the malonamide group were defined to make up the core (see figure 1, green circles). Then a convex hull was laid around those atoms, as seen in figure 6(a), and the area of this hull calculated. Core areas of 196, 197 and 193 $Å^2$ with standard deviations of 4, 3 and 3 $Å^2$ were found for *n*-heptane, *n*-nonane and *n*-dodecane, respectively.

Analogously, the volume of the apolar ring was calculated by forming a convex hull around all atoms of the micelle, computing the volume of the hull and subtracting the volume of the core. Figure 6(b) shows both hulls with projections on the coordinate planes for one frame of the simulation, typically the last one. The corresponding values are 3.2×10^3, 3.1×10^3 and 3.2×10^3 $Å^3$ with standard deviations of 0.3×10^3, 0.3×10^3 and 0.4×10^3 $Å^3$ for *n*-heptane, *n*-nonane and *n*-dodecane, respectively. The projections show that the core and the apolar ring are approximately spherical and fluctuate with an instantaneous ellipticity of approximately 0.25. This is owed to the small aggregation number, which simply makes the interface lack extractant chains to form a spherical aggregate. One may think that

explicitly accounting for the presence of n-alkane molecules in the apolar region of the aggregate (interacting very weakly with the hydrophobic chains of the DMDOHEMA molecule) should make the aggregate fully spherical. However, using our definition of the apolar region, i.e., consisting only of the hydrophobic chains of the DMDOHEMA molecules, we already implicitly took into account a part of the n-alkane molecules penetrating in the apolar region since we calculated the volume of the convex hull. Nevertheless, considering explicitly the presence of n-alkane molecules in the apolar region, which corresponds to another model since the definition of the apolar region is different, changes little the volumes calculated. Indeed, an increase of around 10% is calculated. This will have also an influence on the calculated spontaneous packing parameter and bending rigidity. However, in this case, we have to note that the definition of distance criteria to define wether the n-alkane molecules belong to the apolar region (between the DMDOHEMA and the n-alkane and Eu^{3+} and the n-alkane molecules) are based on non well-defined radial distribution functions. The definition of these criteria is therefore quite complex since very little structuration is observed. Thus, for the rest of the study, we considered only the hydrophobic chains of the DMDOHEMA molecules for the definition of the apolar region.

4.4. Micelle geometry

To validate the assumption of a reverse spherical micelle the geometry of the aggregate was investigated. Therefore, the micelle in n-heptane was projected onto a polar coordination sphere and observed as a function of the simulation time (Fig. 7). The chain atoms are displayed in yellow, green, and blue colors with the core atoms highlighted in red. Atom positions, centered

around the Eu^{3+} cation, were projected for a single frame (1 ps), 100, 1000 and 5000 ps. It was observed that the micelle, indeed, fluctuates around a spherical geometry in a time scale above 1 ns. The same was observed for the micelles in *n*-nonane and *n*-dodecane, where it took increasing times for the micelle to fluctuate. This may be due to the decreased diffusion in *n*-nonane and *n*-dodecane.

4.5. Packing parameter

To obtain the free energy of bending as a function of the packing parameter different approaches based on different definitions of the packing parameter have been used. The energy was either calculated from umbrella sampling (US) molecular dynamics simulations or using fluctuation theory from the classical non-biased molecular dynamics simulations. The packing parameter itself was calculated either directly by Equation 9 or by the modified Equation 10 only depending on the core radius and the chain length. The latter approach is only valid for spherical geometry.

Since the length of the hydrophobic tail is known, the only missing value needed to calculate the packing parameter via Equation 10 is the core radius R. Assuming a triangular geometry of the polar core of the micelle, as in figure 3, where the atoms form the corners of a triangle, the radius of the circle can be calculated as

$$R = \frac{\xi_1 \xi_2 \xi_3}{\sqrt{(\xi_1 + \xi_2 + \xi_3) + (\xi_1 + \xi_2 - \xi_3) + (\xi_2 + \xi_3 - \xi_1) + (\xi_3 + \xi_1 - \xi_2)}}. \tag{11}$$

For the specific case of an equilateral triangle the equation simplifies to

$$R = \bar{\xi}\frac{\sqrt{3}}{3}. \tag{12}$$

Aware of these connections, the three reaction coordinates ξ_1, ξ_2 and ξ_3 can be combined to the average value $\bar{\xi}$ or the radius R. For the sake of simplicity, the WHAM processing was done by considering only one degree of freedom, either $\bar{\xi}$ or R. It has to be noted that due to the parameter reduction adapted spring constants k must be used for the analysis with WHAM. The general perturbation Hamiltonian of the umbrella sampling reads

$$H' = \frac{1}{2}k\sum_{i=1}^{3}(\xi_i - \xi_0)^2 \tag{13}$$

where ξ_0 is the reaction coordinate. If one considers that the geometry remains quasi-symmetric during the simulation, *i.e.*, the three reaction coordinates ξ_1, ξ_2 and ξ_3 are close to the average value $\bar{\xi}$, H' is equivalent to the Hamiltonian with a single spring on the $\bar{\xi}$ parameter but with an effective spring constant $k_{\text{eff}} = 3k$. Once the free energy as a function of $\bar{\xi}$ is obtained, the free energy as a function of p is deduced from Equations 10 and 12. The US calculations can also be done by using the radius R. In that case, for any configuration, the radius R is calculated from Equation 11. Always considering a constant symmetrical geometry, the perturbation Hamiltonian becomes

$$H' = \frac{9}{2}k\left(R - \frac{\xi_0}{\sqrt{3}}\right)^2. \tag{14}$$

Therefore, in that case where the WHAM algorithm is performed with R, the effective spring constant is $k_{\text{eff}} = 9k$. The free energy is finally expressed as a function of p thanks to Equation 10.

Figure 8 shows the PMFs calculated for the approaches using the two US methodologies considering (a) the average distance $\bar{\xi}$ and (b) the radius R (Equation 11). The curves obtained using both approaches are in very good

agreement and validate the approach of parameter reduction for WHAM analysis. In both cases, the spontaneous packing parameter p_0 was found to be 4.6 for *n*-heptane, *n*-nonane and *n*-dodecane. The local minimum to the left of the p_0 corresponds to an aggregate where one DMDOHEMA is in the Eu^{3+} second coordination sphere coordinating to the water molecule. For *n*-dodecane, this configuration seems to have a slightly lower barrier. For even smaller packing parameters –corresponding to larger spherical micelles– *n*-nonane has the lowest potential curve. This may be due to the similarity between the diluent and the DMDOHEMA molecule in terms of chain length (Fig. 4), which is highest for *n*-nonane and therefore may allow a stronger penetration and a swelling of the micelle. For too small core sizes (p values above p_0) the core eventually collapses and counter ions or hydrating water get forced out of the core. With increasing hydrophobicity of the diluent, the stability of those aggregates decreases drastically.

An alternative methodology is to calculate the packing parameter via the fluctuation of the distance between the ternary carbon atoms of the diamide group of DMDOHEMA. The definition of the packing parameter is analogous to the one used in umbrella sampling, but the relevant C4-C4 distances ξ_i were obtained directly from classical MD simulation without any restraints. Figure 9 shows the free energy potentials obtained using such an approach. The spontaneous packing parameters p_0 are found to be 4.5 for *n*-heptane and *n*-nonane, and 4.6 for *n*-dodecane and therefore correspond very well with those calculated using the umbrella sampling approach. Additionally, already a deviation of the parabola is observed for sufficiently large (for *n*-heptane) and small (for *n*-dodecane) p values, corresponding to the area of

a local minimum ($p \approx 4.1$) and the higher stability of large p in n-heptane, compared to figure 8.

In comparison, the packing parameter was calculated using the fluctuating values of the volume v, the head group area a_0 and the chain length L_s via Equation 9 (Fig. 10). This approach has the advantage that it does not explicitly assume the geometry of the aggregate and therefore could be applied to any system whether it is spherical or not. Here, values of 1.8, 1.7 and 1.9 for the p_0 were obtained for n-heptane, n-nonane and n-dodecane, respectively. The values calculated are significantly lower than those of the umbrella sampling method. This is due to the fact that, in the case of the US approach, the micelle was assumed to be spherical in order to get the packing parameter from the reaction coordinate ξ_0, while this method takes the instantaneous geometrical properties into account. As seen in figure 6, the micelle is rather oblate spheroidal and therefore a smaller spontaneous packing parameter is expected.

4.6. Rigidity constants

From the free energy profiles calculated in the n-alkanes the effective bending constants were determined using the molecular formalism from Equation 5. All the constants are found in Table 2.

The yielded rigidity constant depends rather on the definition of the packing parameter than on the methodology used to obtain it. For approaches using the core radius to calculate p, values in the range of 50 $k_\mathrm{B}T$ per extractant molecule were found for all n-alkanes. Solely the fluctuation of the radius produces larger values. It is expected that a longer simulation run will give both a better coincidence of the yielded rigidity constant for US

Table 2: Spontaneous packing parameter p_0 and effective rigidity constant κ^* calculated from the different approaches

	n-heptane		*n*-nonane		*n*-dodecane	
	p_0	$\kappa^{*\,a}$	p_0	$\kappa^{*\,a}$	p_0	$\kappa^{*\,a}$
US $\bar{\xi}$	4.6	50	4.6	51	4.6	50
US R	4.6	49	4.6	48	4.6	47
fluctuation R	4.5	53	4.5	83	4.6	62
fluctuation v	1.8	9	1.7	17	1.9	6

[a] in $k_\mathrm{B}T$ per extractant molecule.

and fluctuation, and a more parabolic energy profile.

Compared to effective bending rigidities found in the literature and calculated for lipid bilayers or microemulsions, *i.e.*, typically in the order of magnitude of a few $k_\mathrm{B}T$ [76–79], these values seem proportionately high. This is due to the nature of the investigated micelles. While in earlier literature mainly water swollen micelles not containing cations and with radii much larger than 10 Å were considered, the simulated aggregate is a very small and rigid reverse micelle owed to the strong interaction with the charged Eu^{3+} cation. The radius of the micelles in all *n*-alkanes was found to be around 4.2 Å. The radii as well as the effective bending rigidities are in good agreement with former investigations of a reverse micelle containing La^{3+} and four DMDOHEMA molecules [52].

With the approaches using the different definition of the packing parameter deviating values were found. The fluctuation of volume and area gives rigidity constants of 9, 17 and 6 $k_\mathrm{B}T$ per extractant molecule for *n*-heptane,

n-nonane and n-dodecane, respectively. It is difficult to put the values in relation to each other because of the fundamentally different approach. However, a longer simulation run is expected to result in a better agreement between the results for different diluents.

5. Conclusion

In the present work, aggregates composed of $Eu(NO_3)_3$, water and the extractant DMDOHEMA diluted in the three n-alkanes, *i.e.*, n-heptane, n-nonane and n-dodecane were simulated using classical molecular dynamics simulations. The fluctuations of the system were investigated from a thermodynamic point of view. Furthermore, external constraints were applied to alter the micelle in a way that did not change the nature of the cation, yet change the micelle surface. Thus, the energy profiles of the aggregate in different diluents became accessible. In the end, the spontaneous packing parameter p_0 and the effective bending rigidity constant κ^* were calculated to investigate whether and, if so, how those parameters were influenced by the diluent. It was found that (a) both, fluctuation theory and umbrella sampling, are valid ways to investigate the energy profiles of small reverse micelle, and (b) the diluent has a minor effect on the spontaneous packing parameter and the effective bending rigidity. The energy profiles in the different n-alkanes coincide around the local minimum p_0, while outside this region they mainly differ.

This work validates the approach using fluctuation theory as a way to investigate the energy profiles of a system analogous to umbrella sampling, while being less time and work consuming. Furthermore, such an approach

has the advantage that it does not depend on the geometry of the aggregate formed so that it can be applied to any system whether it is spherical or not. In this work only unbranched diluents were used, but it is expected that branched diluents exhibit a significantly different penetration behavior and, therefore, alter the micelle parameters drastically. Understanding the influence of the diluent on the micelle parameters both, paves the way for a better understanding of the underlying thermodynamics and directly benefits the application in the extraction of metal ions. But to make it, more research on additional systems has to be done.

Acknowledgements

The authors thank ANR MULTISEPAR (ANR-18-CE29-0010) for financial support. The authors thank also the referees for their relevant and fruitful remarks.

References

[1] L. Berthon, F. Testard, L. Martinet, T. Zemb, C. Madic, Influence of the extracted solute on the aggregation of malonamide extractant in organic phases: Consequences for phase stability, C. R. Chimie 13 (10) (2010) 1326–1334.

[2] R. J. Ellis, Y. Meridiano, J. Muller, L. Berthon, P. Guilbaud, N. Zorz, M. R. Antonio, T. Demars, T. Zemb, Complexation-induced supramolecular assembly drives metal-ion extraction, Chem. – Eur. J. 20 (40) (2014) 12796–12807.

[3] F. W. Lewis, L. M. Harwood, M. J. Hudson, A. Geist, V. N. Kozhevnikov, P. Distler, J. John, Hydrophilic sulfonated bis-1,2,4-triazine ligands are highly effective reagents for separating actinides(III) from lanthanides(III) via selective formation of aqueous actinide complexes, Chem. Sci. 6 (2015) 4812–4821.

[4] M. Špadina, K. Bohinc, T. Zemb, J.-F. Dufrêche, Synergistic solvent extraction is driven by entropy, ACS Nano 13 (12) (2019) 13745–13758.

[5] Z. Liang, W. Bu, K. J. Schweighofer, D. J. Walwark, J. S. Harvey, G. R. Hanlon, D. Amoanu, C. Erol, I. Benjamin, M. L. Schlossman, Nanoscale view of assisted ion transport across the liquid–liquid interface, Proc. Natl. Acad. Sci. USA 116 (37) (2019) 18227–18232.

[6] M. Gradzielski, M. Duvail, P. M. de Molina, M. Simon, Y. Talmon, T. Zemb, Using microemulsions: Formulation based on knowledge of their mesostructure, Chem. Rev. 121 (10) (2021) 5671–5740.

[7] R. J. Ellis, M. R. Antonio, Coordination structures and supramolecular architectures in a cerium(III)-malonamide solvent extraction system, Langmuir 28 (14) (2012) 5987–5998.

[8] P. Guilbaud, T. Zemb, Depletion of water-in-oil aggregates from poor solvents: Transition from weak aggregates towards reverse micelles, Curr. Opin. Colloid Interface Sci. 20 (1) (2015) 71–77.

[9] D. Jagleniec, Ł. Dobrzycki, M. Karbarz, J. Romański, Ion-pair induced supramolecular assembly formation for selective extraction and sensing of potassium sulfate, Chem. Sci. 10 (2019) 9542–9547.

[10] H. F. Eicke, H. Christen, Nucleation process of micelle formation in apolar solvents, J. Colloid Interface Sci. 48 (2) (1974) 281–290.

[11] B. Qiao, G. Ferru, M. Olvera de la Cruz, R. J. Ellis, Molecular origins of mesoscale ordering in a metalloamphiphile phase, ACS Cent. Sci. 1 (9) (2015) 493–503.

[12] L. J. White, N. J. Wells, L. R. Blackholly, H. J. Shepherd, B. Wilson, G. P. Bustone, T. J. Runacres, J. R. Hiscock, Towards quantifying the role of hydrogen bonding within amphiphile selfaassociation and resultant aggregate formation, Chem. Sci. 8 (2017) 7620–7630.

[13] R. Motokawa, T. Kobayashi, H. Endo, J. Mu, C. D. Williams, A. J. Masters, M. R. Antonio, W. T. Heller, M. Nagao, A telescoping view of solute architectures in a complex fluid system, ACS Cent. Sci. 5 (1) (2019) 85–96.

[14] W. H. Duan, Q. Wang, F. Collins, Dispersion of carbon nanotubes with sds surfactants: a study from a binding energy perspective, Chem. Sci. 2 (2011) 1407–1413.

[15] H. Kumari, S. R. Kline, J. L. Atwood, Aqueous solubilization of hydrophobic supramolecular metal–organic nanocapsules, Chem. Sci. 5 (2014) 2554–2559.

[16] H. Zhang, K. Dasbiswas, N. B. Ludwig, G. Han, B. Lee, S. Vaikuntanathan, D. V. Talapin, Stable colloids in molten inorganic salts, Nature 542 (2017) 328–331.

[17] T. Wei, C. Chen, J. Liu, C. Liu, P. Posocco, X. Liu, Q. Cheng, S. Huo, Z. Liang, M. Fermeglia, S. Pricl, X.-J. Liang, P. Rocchi, L. Peng, Anticancer drug nanomicelles formed by self-assembling amphiphilic dendrimer to combat cancer drug resistance, Proc. Natl. Acad. Sci. USA 112 (10) (2015) 2978–2983.

[18] B. Abécassis, F. Testard, T. Zemb, L. Berthon, C. Madic, Effect of n-octanol on the structure at the supramolecular scale of concentrated dimethyldioctylhexylethoxymalonamide extractant solutions, Langmuir 19 (17) (2003) 6638–6644.

[19] L. Berthon, L. Martinet, F. Testard, C. Madic, T. Zemb, Solvent penetration and sterical stabilization of reverse aggregates based on the diamex process extracting molecules: Consequences for the third phase formation, Solvent Extr. Ion Exch. 25 (5) (2007) 545–576.

[20] D. Serrano-Purroy, P. Baron, B. Christiansen, R. Malmbeck, C. Sorel, J. P. Glatz, Recovery of minor actinides from hllw using the diamex process, Radiochim. Acta 93 (6) (2005) 351–355.

[21] G. Modolo, H. Vijgen, D. Serrano-Purroy, B. Christiansen, R. Malmbeck, C. Sorel, P. Baron, Diamex counter-current extraction process for recovery of trivalent actinides from simulated high active concentrate, Sep. Sci. Technol. 42 (3) (2007) 439–452.

[22] B. Gannaz, R. Chiarizia, M. R. Antonio, C. Hill, G. Cote, Extraction of lanthanides(III) and Am(III) by mixtures of malonamide and dialkkyphosphoric acid, Solvent Extr. Ion Exch. 25 (3) (2007) 313–337.

[23] Y. Meridiano, L. Berthon, X. Crozes, C. Sorel, P. Dannus, M. R. Antonio, R. Chiarizia, T. Zemb, Aggregation in organic solutions of malonamides: Consequences for water extraction, Solvent Extr. Ion Exch. 27 (5-6) (2009) 607–637.

[24] R. J. Ellis, Y. Meridiano, R. Chiarizia, L. Berthon, J. Muller, L. Couston, M. R. Antonio, Periodic behavior of lanthanide coordination within reverse micelles, Chem. – Eur. J. 19 (8) (2013) 2663–2675.

[25] M. R. Antonio, R. Chiarizia, B. Gannaz, L. Berthon, N. Zorz, C. Hill, G. Cote, Aggregation in solvent extraction systems containing a malonamide, a dialkylphosphoric acid and their mixtures, Sep. Sci. Technol. 43 (9-10) (2008) 2572–2605.

[26] B. Qiao, T. Demars, M. Olvera De La Cruz, R. J. Ellis, How hydrogen bonds affect the growth of reverse micelles around coordinating metal ions, J. Phys. Chem. Lett. 5 (8) (2014) 1440–1444.

[27] B. Qiao, G. Ferru, R. J. Ellis, Complexation enhancement drives water-to-oil ion transport: A simulation study, Chem. – Eur. J. 23 (2) (2017) 427–436.

[28] C. Erlinger, D. Gazeau, T. Zemb, C. Madic, L. Lefrançois, M. Hebrant, C. Tondre, Effect of nitric acid extraction on phase behavior, microstructure and interactions between primary aggregates in the system dimethyldibutyltetradecylmalonamide (DMDBTDMA) / n-dodecane / water: A phase analysis and small angle x-ray scattering (SAXS) characterisation study, Solvent Extr. Ion Exch. 16 (3) (1998) 707–738.

[29] T. Sukhbaatar, M. Duvail, T. Dumas, S. Dourdain, G. Arrachart, P. L. Solari, P. Guilbaud, S. Pellet-Rostaing, Probing the existence of uranyl trisulfate structures in the amex solvent extraction process, Chem. Commun. 55 (2019) 7583–7586.

[30] X. Ye, S. Cui, V. F. de Almeida, B. P. Hay, B. Khomami, Uranyl nitrate complex extraction into TBP/dodecane organic solutions: a molecular dynamics study, Phys. Chem. Chem. Phys. 12 (2010) 15406–15409.

[31] M. B. Singh, A. J. Mukhtyar, Y. Z. Bootwala, V. G. Gaikar, Extraction of cadmium by TODGA–dodecane and TBP–dodecane: A comparative study by MD simulation, Sep. Sci. Technol. 52 (7) (2017) 1172–1185.

[32] J. J. Karnes, N. Villavicencio, I. Benjamin, Transfer of an erbium ion across the water/dodecane interface: Structure and thermodynamics via molecular dynamics simulations, Chem. Phys. Lett. 737 (2019) 136825.

[33] D. Moreno Martinez, E. Acher, M. Vatin, S. Dourdain, D. Guillaumont, P. Guilbaud, Aggregation of bifunctional extractants used for uranium(VI) separation, J. Phys. Chem. B 125 (38) (2021) 10759–10771.

[34] J.-F. Dufrêche, T. Zemb, Effect of long-range interactions on ion equilibria in liquid–liquid extraction, Chem. Phys. Lett. 622 (2015) 45–49.

[35] M. Špadina, J.-F. Dufrêche, S. Pellet-Rostaing, S. Marčelja, T. Zemb, Molecular forces in liquid–liquid extraction, Langmuir 37 (36) (2021) 10637–10656.

[36] J.-F. Dufrêche, T. Zemb, Bending: from thin interfaces to molecular

films in microemulsions, Curr. Opin. Colloid Interface Sci. 49 (2020) 133–147.

[37] M. Bley, B. Siboulet, A. Karmakar, T. Zemb, J.-F. Dufrêche, A predictive model of reverse micelles solubilizing water for solvent extraction, J. Colloid Interface Sci. 479 (2016) 106–114.

[38] A. Karmakar, M. Duvail, M. Bley, T. Zemb, J.-F. Dufrêche, Combined supramolecular and mesoscale modelling of liquid–liquid extraction of rare earth salts, Colloids Surfaces A Physicochem. Eng. Asp. 555 (2018) 713–727.

[39] M. Špadina, K. Bohinc, T. Zemb, J.-F. Dufrêche, Multicomponent model for the prediction of nuclear waste/rare-earth extraction processes, Langmuir 34 (35) (2018) 10434–10447.

[40] M. Špadina, K. Bohinc, T. Zemb, J.-F. Dufrêche, Colloidal model for the prediction of the extraction of rare earths assisted by the acidic extractant, Langmuir 35 (8) (2019) 3215–3230.

[41] S. Gourdin-Bertin, J.-F. Dufrêche, M. Duvail, T. Zemb, Microemulsion as model to predict free energy of transfer of electrolyte in solvent extraction, Solvent Extr. Ion Exch. In Press (2021) 1–36. doi:10.1080/07366299.2021.1953259.

[42] M. J. Servis, G. B. Stephenson, Mesostructuring in liquid–liquid extraction organic phases originating from critical points, J. Phys. Chem. Lett. 12 (24) (2021) 5807–5812.

[43] M. Vatin, M. Duvail, P. Guilbaud, J.-F. Dufrêche, Thermodynamics of malonamide aggregation deduced from molecular dynamics simulations, J. Phys. Chem. B 125 (13) (2021) 3409–3418.

[44] M. Pleines, W. Kunz, T. Zemb, D. Benczédi, W. Fieber, Molecular factors governing the viscosity peak of giant micelles in the presence of salt and fragrances, J. Colloid Interface Sci. 537 (2019) 682–693.

[45] K. D. Danov, P. A. Kralchevsky, S. D. Stoyanov, J. L. Cook, I. P. Stott, E. G. Pelan, Growth of wormlike micelles in nonionic surfactant solutions: Quantitative theory vs. experiment, Adv. Colloid Interface Sci. 256 (2018) 1–22.

[46] K. D. Danov, P. A. Kralchevsky, R. D. Stanimirova, S. D. Stoyanov, J. L. Cook, I. P. Stott, Analytical modeling of micelle growth. 4. molecular thermodynamics of wormlike micelles from ionic surfactants: Theory vs. experiment, J. Colloid Interface Sci. 584 (2021) 561–581.

[47] W. Helfrich, Elastic properties of lipid bilayers: Theory and possible experiments, Z. Naturforsch., C: J. Biosci. 28 (11-12) (1973) 693–703.

[48] L. Szleifer, D. Kramer, A. Ben-Shaul, W. M. Gelbart, S. A. Safran, Molecular theory of curvature elasticity in surfactant films, J. Chem. Phys. 92 (11) (1990) 6800–6817.

[49] P. Pieruschka, S. A. Safran, Random Interfaces and the Physics of Microemulsions, Europhys. Lett. 22 (8) (1993) 625–630.

[50] P. Pieruschka, S. A. Safran, A random interface model of microemulsions, J. Phys.: Condens. Matter 6 (23A) (1994) A357–A362.

[51] L. Arleth, S. Marčelja, T. Zemb, Gaussian random fields with two level-cuts - Model for asymmetric microemulsions with nonzero spontaneous curvature?, J. Chem. Phys. 115 (8) (2001) 3923–3936.

[52] M. Duvail, S. Van Damme, P. Guilbaud, Y. Chen, T. Zemb, J. F. Dufrêche, The role of curvature effects in liquid-liquid extraction: Assessing organic phase mesoscopic properties from MD simulations, Soft Matter 13 (33) (2017) 5518–5526.

[53] J. N. Israelachvili, D. J. Mitchell, B. W. Ninham, Theory of self-assembly of hydrocarbon amphiphiles into micelles and bilayers, J. Chem. Soc., Faraday Trans. 72 (1976) 1525–1568.

[54] D. A. Case, V. Babin, J. T. Berryman, R. M. Betz, Q. Cai, D. S. Cerutti, T. E. Cheatham, III, T. A. Darden, R. E. Duke, H. Gohlke, A. W. Goetz, S. Gusarov, N. Homeyer, P. Janowski, J. Kaus, I. Kolossváry, A. Kovalenko, T. S. Lee, S. LeGrand, T. Luchko, R. Luo, B. Madej, K. M. Merz, F. Paesani, D. R. Roe, A. Roitberg, C. Sagui, R. Salomon-Ferrer, G. Seabra, C. L. Simmerling, W. Smith, J. Swails, R. C. Walker, J. Wang, R. M. Wolf, X. Wu, P. Kollman, AMBER 14, University of California, San Francisco (2014).
URL `http://ambermd.org/`

[55] M. Duvail, M. Souaille, R. Spezia, T. Cartailler, P. Vitorge, Pair interaction potentials with explicit polarization for molecular dynamics simulations of La^{3+} in bulk water, J. Chem. Phys. 127 (3) (2007) 034503–11.

[56] M. Duvail, P. Vitorge, R. Spezia, Building a polarizable pair interaction

potential for lanthanoids(III) in liquid water: A molecular dynamics study of structure and dynamics of the whole series, J. Chem. Phys. 130 (10) (2009) 104501–13.

[57] M. Duvail, A. Ruas, L. Venault, P. Moisy, P. Guilbaud, Molecular dynamics studies of concentrated binary aqueous solutions of lanthanide salts: Structures and exchange dynamics, Inorg. Chem. 49 (2) (2010) 519–530.

[58] Y. Chen, M. Duvail, P. Guilbaud, J. F. Dufrêche, Stability of reverse micelles in rare-earth separation: A chemical model based on a molecular approach, Phys. Chem. Chem. Phys. 19 (10) (2017) 7094–7100.

[59] M. Diaz Peña, G. Tardajos, R. Arenosa, C. Menduiña, Isothermal compressibility of benzene + n-undecane, + n-dodecane, + n-tetradecane, and + n-hexadecane, J. Chem. Thermodyn. 11 (10) (1979) 951 – 957.

[60] A. T. Balaban, N. H. March, D. J. Klein, Relation of surface tension to compressibility at room temperature and wetting index also involving viscosity for 22 organic liquids, Phys. Chem. Liq. 47 (1) (2009) 1–4.

[61] T. Darden, D. York, L. Pedersen, Particle Mesh Ewald: An $N \cdot \log(N)$ Method for Ewald Sums in Large Systems, J. Chem. Phys. 98 (12) (1993) 10089–10092.

[62] J. W. Caldwell, P. A. Kollman, Structure and properties of neat liquids using nonadditive molecular dynamics: Water, methanol, and n-methylacetamide, J. Phys. Chem. 99 (16) (1995) 6208–6219.

[63] E. C. Meng, P. A. Kollman, Molecular dynamics studies of the properties of water around simple organic solutes, J. Phys. Chem. 100 (27) (1996) 11460–11470.

[64] M. Duvail, P. Guilbaud, Understanding the nitrate coordination to Eu^{3+} ions in solution by potential of mean force calculations, Phys. Chem. Chem. Phys. 13 (13) (2011) 5840–5847.

[65] M. Duvail, T. Dumas, A. Paquet, A. Coste, L. Berthon, P. Guilbaud, UO_2^{2+} structure in solvent extraction phases resolved at molecular and supramolecular scales: a combined molecular dynamics, EXAFS and SWAXS approach, Phys. Chem. Chem. Phys. 21 (2019) 7894–7906.

[66] S. W. I. Siu, K. Pluhackova, R. A. Böckmann, Optimization of the opls-aa force field for long hydrocarbons, J. Chem. Theory. Comp. 8 (4) (2012) 1459–1470.

[67] P. T. van Duijnen, M. Swart, Molecular and atomic polarizabilities: Thole's model revisited, J. Phys. Chem. A 102 (14) (1998) 2399–2407.

[68] W. Humphrey, A. Dalke, K. Schulten, Vmd: Visual molecular dynamics, J. Mol. Graph. 14 (1) (1996) 33–38.

[69] D. R. Roe, T. E. Cheatham, Ptraj and cpptraj: Software for processing and analysis of molecular dynamics trajectory data, J. Chem. Theory Comput. 9 (7) (2013) 3084–95.

[70] N. Michaud-Agrawal, E. J. Denning, T. B. Woolf, O. Beckstein, MD-Analysis: A toolkit for the analysis of molecular dynamics simulations, J. Comput. Chem. 32 (10) (2011) 2319–2327.

[71] R. J. Gowers, M. Linke, J. Barnoud, T. J. E. Reddy, M. N. Melo, S. L. Seyler, J. Domański, D. L. Dotson, S. Buchoux, I. M. Kenney, O. Beckstein, MDAnalysis: A Python Package for the Rapid Analysis of Molecular Dynamics Simulations, in: S. Benthall, S. Rostrup (Eds.), Proceedings of the 15th Python in Science Conference, 2016, pp. 98–105.

[72] T. E. Oliphant, Python for scientific computing, Comput. Sci. Eng. 9 (3) (2007) 10–20.

[73] A. Grossfield, Wham: the weighted histogram analysis method, version 2.09 (2015).

[74] S. Kumar, J. M. Rosenberg, D. Bouzida, R. H. Swendsen, P. A. Kollman, Multidimensional free-energy calculations using the weighted histogram analysis method, J. Comput. Chem. 16 (11) (1995) 1339–1350.

[75] C. Tanford, Micelle shape and size, J. Phys. Chem. 76 (21) (1972) 3020–3024.

[76] B. P. Binks, J. Meunier, O. Abillon, D. Langevin, Measurement of film rigidity and interfacial tensions in several ionic surfactant-oil-water microemulsion systems, Langmuir 5 (2) (1989) 415–421.

[77] B. Farago, D. Richter, J. S. Huang, S. A. Safran, S. T. Milner, Shape and size fluctuations of microemulsion droplets: The role of cosurfactant, Phys. Rev. Lett. 65 (26) (1990) 3348–3351.

[78] T. Hellweg, D. Langevin, Bending elasticity of the surfactant monolayer in droplet microemulsions: Determination by a combination of dynamic

light scattering and neutron spin-echo spectroscopy, Phys. Rev. E 57 (6) (1998) 6825–6834.

[79] O. Holderer, H. Frielinghaus, M. Monkenbusch, M. Klostermann, T. Sottmann, D. Richter, Experimental determination of bending rigidity and saddle splay modulus in bicontinuous microemulsions, Soft Matter 9 (7) (2013) 2308–2313.

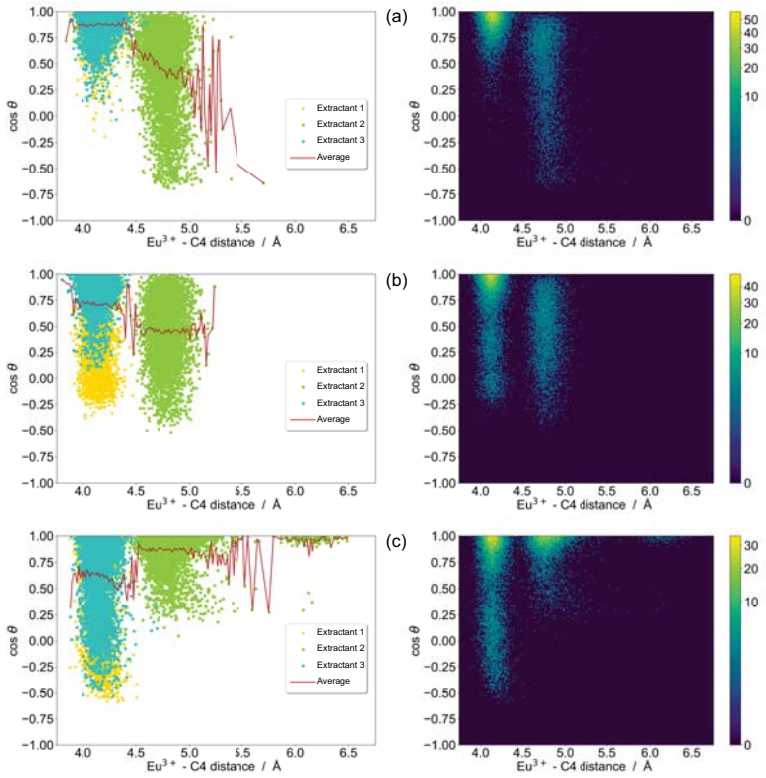

Figure 5: (Left) Cosine of the angle between the terminal carbon of the hexyl-ethoxy chain of DMDOHEMA and the Eu-C4 distance as a function of the Eu-C4 distance in (a) *n*-heptane, (b) *n*-nonane, and (c) *n*-dodecane. Color points (yellow, green, and blue) represent the three DMDOHEMA molecules. The red line is the average cosine of angle calculated over the three DMDOHEMA molecules. (Right) Corresponding histograms where the color bar corresponds to an arbitrary scaled probability.

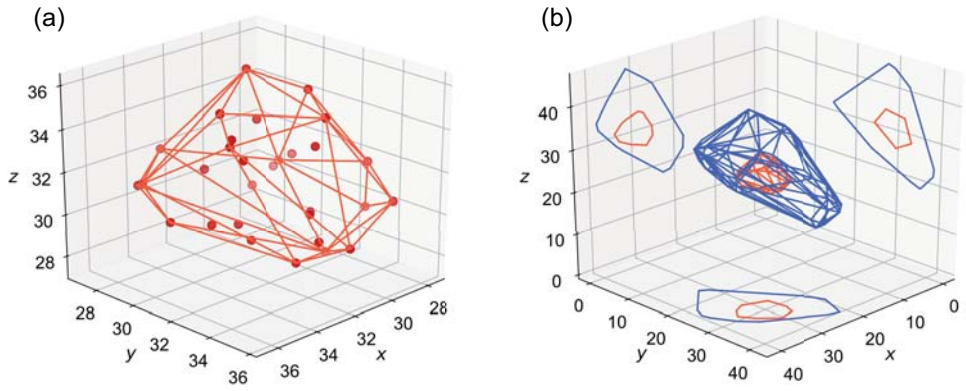

Figure 6: (a) Convex hull around the polar core for the micelle in *n*-heptane. The red lines depict the edges of the hull around the atoms defined to build up the core (red dots). (b) Convex hull around apolar ring (blue lines) and polar core (red lines). Projections on the yz, xz and xy planes show the geometry of the hulls and their relative position to each other.

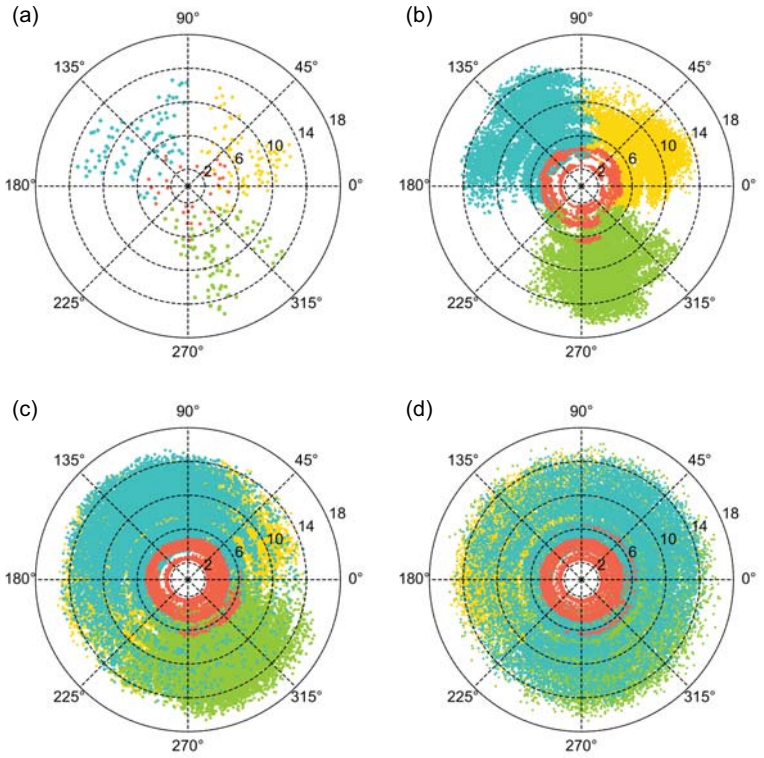

Figure 7: Projections of the atoms making up the micelle in *n*-heptane onto a polar coordinate system for (a) one simulation frame (1 ps), (b) 100 ps, (c) 1 ns and (d) 5 ns. Atoms that were declared as core atoms (see figure 1) are depicted in red, all remaining atoms are in yellow, green, and blue colors corresponding to DMDOHEMA 1, 2, and 3, respectively. Distances to Eu^{3+}cation (in Å) are also shown as subcircles.

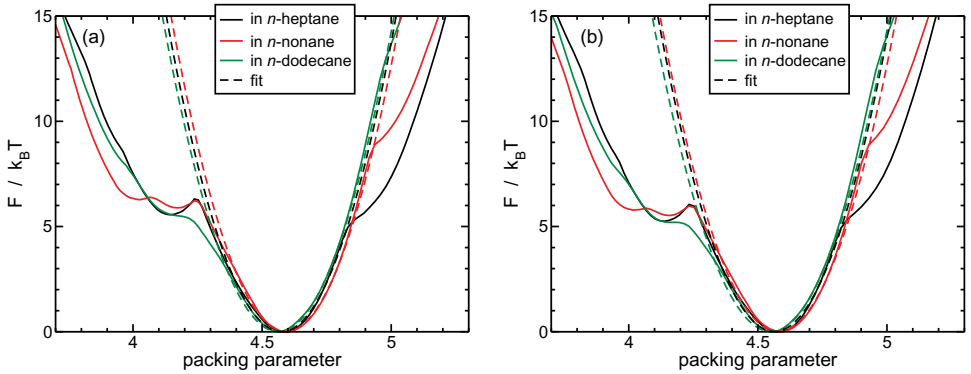

Figure 8: Potential of mean force profiles calculated from umbrella sampling molecular dynamics simulations as a function of the packing parameter p in n-heptane (black), n-nonane (red) and n-dodecane (green). The dashed lines show the parabolic fit near the minimum p_0. The weighted histogram was calculated from (a) the average C4-C4 distance $\bar{\xi}$ or (b) the radius calculated from the three distinct C4-C4 distances ξ_i.

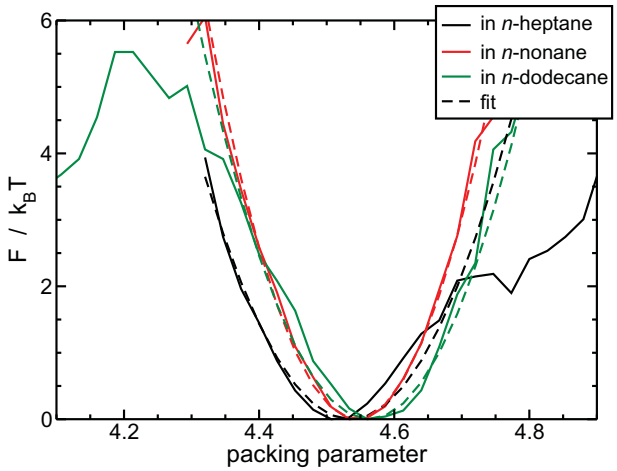

Figure 9: Free energy of the micelle as a function of the packing parameter calculated from fluctuating ξ_i distances. The dashed lines show the parabolic fit near the minimum p_0.

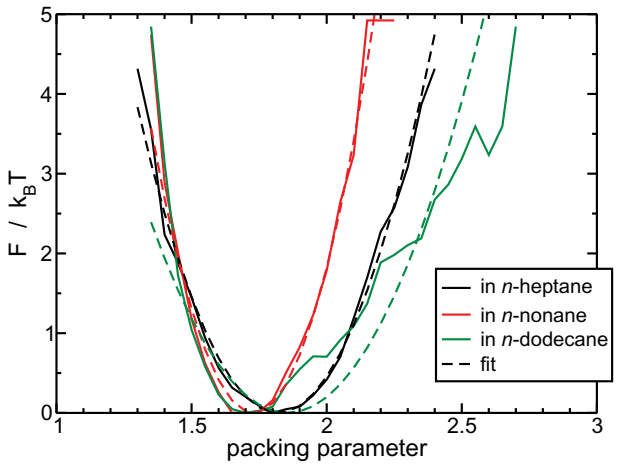

Figure 10: Free energy of the micelle as a function of the packing parameter calculated from fluctuating core area and micelle volume.

Declaration of interests

☒ The authors declare that they have no known competing financial interests or personal relationships that could have appeared to influence the work reported in this paper.

☐The authors declare the following financial interests/personal relationships which may be considered as potential competing interests:

Graphical Abstract

Molecular dynamics simulations of $Eu(NO_3)_3$ salt with DMDOHEMA in n-alkanes: Unravelling curvature properties in liquid-liquid extraction

Simon Stemplinger, Magali Duvail, Jean-François Dufrêche

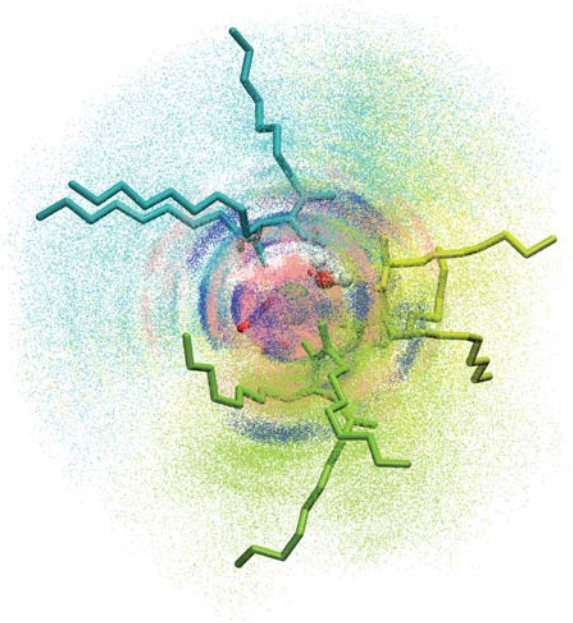

A new molecular dynamics approach for investigating the curvature properties of reverse micelles involved in liquid-liquid extraction.